Potential Precipitation Predictability Decreases Under Future Warming

Article *in* Geophysical Research Letters · November 2020

DOI: 10.1029/2020GL090798

CITATIONS
13

READS
496

6 authors, including:

Lei Xu
China University of Geosciences
49 PUBLICATIONS **1,778** CITATIONS
SEE PROFILE

Chong Zhang
Capital Normal University
27 PUBLICATIONS **934** CITATIONS
SEE PROFILE

Nengcheng Chen
Wuhan University
236 PUBLICATIONS **4,191** CITATIONS
SEE PROFILE

Moradkhani Hamid
University of Alabama
286 PUBLICATIONS **13,121** CITATIONS
SEE PROFILE

Geophysical Research Letters

RESEARCH LETTER
10.1029/2020GL090798

Potential Precipitation Predictability Decreases Under Future Warming

Lei Xu[1], Chong Zhang[2,3], Nengcheng Chen[1,4], Hamid Moradkhani[2], Pao-Shin Chu[5], and Xiang Zhang[1]

[1]State Key Laboratory of Information Engineering in Surveying, Mapping, and Remote Sensing, Wuhan University, Wuhan, China, [2]Center for Complex Hydrosystems Research, Department of Civil, Construction and Environmental Engineering, University of Alabama, Tuscaloosa, AL, USA, [3]Institute of Land Surface System and Sustainable Development, Beijing Normal University, Beijing, China, [4]Collaborative Innovation Center of Geospatial Technology, Wuhan, China, [5]Department of Atmospheric Sciences, School of Ocean and Earth Science and Technology, University of Hawai'i at Mānoa, Honolulu, HI, USA

Key Points:
- Potential precipitation predictability changes are divergent among different models under future warming
- Predictability is estimated to decrease 0.8%, 0.1%, and 0.3% per 1° rise in global SST for tropical, extratropical areas and globally, respectively
- The decreasing predictability is closely related to the increasing SST and the decrease of potential SST predictability under future warming

Supporting Information:
- Supporting Information S1

Correspondence to:
X. Zhang,
zhangxiangsw@whu.edu.cn

Citation:
Xu, L., Zhang, C., Chen, N., Moradkhani, H., Chu, P.-S., & Zhang, X. (2020). Potential precipitation predictability decreases under future warming. *Geophysical Research Letters*, *47*, e2020GL090798. https://doi.org/10.1029/2020GL090798

Received 11 SEP 2020
Accepted 21 OCT 2020
Accepted article online 29 OCT 2020

Abstract Precipitation predictability is likely to decrease with water cycle intensification under global warming, yet how much it will change spatiotemporally is unclear. We quantify the precipitation predictability changes under future warming using model simulations from Coupled Model Intercomparison Project Phase 5. The global-averaged potential precipitation predictability (PPP) is likely to decrease 0.3% per 1°C increase of global sea surface temperature (SST), with a decrease of 0.8% and 0.1% in tropical and extratropical regions, respectively, under future warming scenarios. The PPP changes are divergent among different models with considerable uncertainty. The estimated declining PPP is closely related to the increase of SST and the decrease of potential SST predictability based on a statistical regression analysis. These results unravel the changing pattern of precipitation predictability under future warming.

Plain Language Summary Precipitation prediction for several weeks or months in advance provides opportunities for the preparation of extreme weather events such as droughts and floods. The predictable ability of precipitation determines how long it can be forecasted. We found that precipitation is becoming more difficult to predict when the global sea surface temperature (SST) continues to increase in the future, although different models show divergent results. The decreasing precipitation predictable ability is well explained by the increasing SST and the decreasing predictable ability of SST. Although extreme precipitation events may increase in a warmer world in the context of the enhanced SST variability and other changes such as sulfate aerosols and land use, precipitation is probably less predictable as a result of lower predictable ability of SST.

1. Introduction

Precipitation is a key climatic variable influencing global water cycle and Earth's energy budgets. Accurate precipitation forecasting is vital for early drought warning, flooding preparation, and water resources management (Hao et al., 2014; Hartmann et al., 2016; Silvestro & Rebora, 2014). The predictability of precipitation is assumed as the limit of predictable ability for a given lead time. The classic predictability measures the reproducing ability of predictands by predictors. Precipitation predictability cannot be directly obtained as precipitation is influenced by numerous factors. Potential predictability (G. J. Boer, 2004) is another way to quantify predictability from a variance fraction perspective. It describes the fraction of long-term variability that may be distinguished from the internally generated natural variability which is not predictable on long time scales and therefore may be considered as "noise." Potential predictability is similar to signal-to-noise ratio and describes the potential predictable ability, which is widely used to evaluate the precipitation predictability in previous studies (G. Boer, 2009; G. Boer & Lambert, 2008; Kang et al., 2004; Lou et al., 2019; W. Wei et al., 2017). Therefore, potential precipitation predictability (PPP) is introduced to estimate precipitation predictability over global lands.

The accuracy of precipitation prediction varies with regions, models, and time scales (Papacharalampous et al., 2018; Xu et al., 2018). Precipitation predictability is generally higher in tropical than extratropical regions because of deep convection in the tropics (Koster et al., 2000; S. Li & Robertson, 2015; Westra & Sharma, 2010; Wheeler et al., 2017; Zhu et al., 2014). Two significant tropical climate patterns, that is, EI

Niño–Southern Oscillation (ENSO) and Madden-Julian Oscillation (MJO), contribute largely to precipitation predictability at subseasonal to seasonal time scales (DelSole et al., 2017; Koster et al., 2000; Westra & Sharma, 2010). Both statistical approaches and dynamic climate models are commonly used to evaluate precipitation predictability (G. Boer & Lambert, 2008; DelSole et al., 2017; Papacharalampous et al., 2018; Wheeler et al., 2017; Xu et al., 2018). As for the predictability in the future, the Coupled Model Intercomparison Project Phase 5 (CMIP5) (Taylor et al., 2012) includes numerous climate simulations under a variety of warming scenarios. Precipitation is predictable over 2 weeks mainly over tropical areas due to low-frequency climate variability (S. Li & Robertson, 2015), and the predictability decreases with the increase of lead time (Wheeler et al., 2017; Zhu et al., 2014).

The weather and climate predictability is likely to decrease under future global warming (G. Boer, 2009; DelSole et al., 2014; S. Li et al., 2020). It is projected that precipitation variability will increase in a warmer world (Pendergrass et al., 2017). However, precipitation predictability is dependent not only on the variability of climatology but also on the variability over different time scales. A recent study concludes that the minimum PPP will increase under future warming based on persistence method (Giorgi et al., 2019). Some studies found that precipitation predictability may not decrease because of new emerging teleconnections under recent global warming (Mamalakis et al., 2018; Wang et al., 2015). Decadal precipitation predictability is likely to decrease under future warming based on climate model simulations (G. Boer, 2009). Therefore, how the PPP will change at subseasonal to seasonal time scales under future warming deserves further study (Dong et al., 2018; Jiang et al., 2016; B. Kirtman et al., 2013; Scher & Messori, 2019).

Sea surface temperature (SST) is a key indicator of global warming and a key driver of global extreme precipitation (R. P. Allan & Soden, 2008; X. Zhou & Khairoutdinov, 2017). SST anomaly is the major precursor of tropical precipitation variability (Liu et al., 2018; Mamalakis et al., 2018) and modulates numerous climate patterns with underlying precipitation predictors such as the MJO (Maloney & Kiehl, 2002). The global-averaged SST is projected to increase ~3°C by 2,100 relative to preindustrial time based on the Intergovernmental Panel on Climate Change (IPCC) Fifth report (Pachauri et al., 2014). How the warming SST influences precipitation predictability has not been consistently concluded (G. Boer, 2009; Giorgi et al., 2019; Luo et al., 2010; Wang et al., 2015).

Unraveling how the precipitation predictability changes with warming SST will provide theoretical support for future weather and climate forecasting. How the PPP change varies with warming levels, regions, and temporal scales is yet to be clarified. To answer these questions, we use CMIP5 models to investigate the PPP changes under future warming relative to preindustrial time. The spatiotemporal patterns of PPP changes at 2-week, 1-month, 2-month, and 3-month time scales are examined over global lands. We also discuss the underlying reasons causing PPP change, with focus on SST and its predictability.

2. Methodology and Data

PPP describes the underlying precipitation predictability in principle (G. J. Boer, 2004). It is expressed as the ratio of long-term precipitation variance by the climatological variance. The climatological variance is calculated on a daily scale over different full periods, and the long-term variance is calculated on 2-week, 1-month, 2-month, and 3-month time scales. If the long-term precipitation variance is distinguishable from climatological variance, the precipitation at long-term scales is potentially predictable. A detailed calculation procedure of the potential predictability variance fraction (ppvf) method is referenced to G. J. Boer (2004).

$$\mathrm{PPP} = \frac{\sigma_L^2}{\sigma^2} \tag{1}$$

where σ_L^2 denotes the long-term variance, obtained through a low-pass filtering averaged over long-term interval, and σ^2 is the climatological variance using daily data. To illustrate this point, let us take the following example, the long-term variance for 1-month time scale is calculated by first averaging the data over each 1-month data concatenation without overlapping and then calculating the variance of the 1-month averaged data. The climatological variance is obtained by the variance of the daily data over different full periods separately, for example, the preindustrial period or the future warming period, because

the climatology may change with period. A PPP value close to zero indicates little predictability, and a value close to one represents high predictability.

A total of 12 CMIP5 (Taylor et al., 2012) models is used to simulate the precipitation predictability at preindustrial control (PiControl), Historical, Representative Concentration Pathway (RCP) 2.6, RCP4.5, and RCP8.5 warming scenarios (Table S1 in the supporting information). The PiControl experiments from 1850 to 1899 (P1) are assumed as preindustrial simulations. Historical simulations from 1956 to 2005 (P2) are used to represent the historical scenario. The CMIP5 simulations from 2051 to 2100 (P3) are adopted as future simulations. A single model simulation may have large uncertainty, while an ensemble of model simulations can reduce the predictability uncertainty to some degree. We calculate the PPP for each individual model first to obtain an ensemble of PPPs and then calculate the mean, median, and other statistics using the ensemble of PPPs. The SST variable from these CMIP5 models is used to calculate the global ocean warming trend and potential SST predictability (PSSTP) using the same ppvf method as PPP (Equation 1).

The historical and RCP8.5 simulations from 1980 to 2019 (P4) are used to calculate the absolute PPP under recent global warming and then compared with observations. The observed precipitation data set from Modern-Era Retrospective analysis for Research and Applications Version 2 (MERRA-2) data (Gelaro et al., 2017) was used to calculate the PPP in the P4 period. The precipitation data from MERRA-2 have overall good performance compared to several reanalysis or interpolated data (Xu et al., 2020). All the data are regridded into daily $5° \times 5°$ resolution. We use a quadratic polynomial to fit the relationship between precipitation or SST and time in a specific period and remove the quadratic trend by keeping the residuals. A multiyear average of the daily precipitation or SST data set is regarded as seasonal impact on predictability and is removed by subtracting it from the entire precipitation or SST data set. The detrending process was conducted before the seasonality removal procedure.

3. Results and Discussion

3.1. Observed and Simulated Precipitation Predictability

Figure 1 plots the absolute PPP obtained from observations and models. The simulated PPP averaged over global lands is consistent with observations (Figure 1a). The observed PPP is well within the bound of simulations. The observed and simulated PPPs decrease from 2-week to 3-month time scales. The observed PPP is consistent with ensemble simulations in the tropical regions (23.5°S to 23.5°N, Figure 1b). For the extratropical regions (south of 23.5°S and north of 23.5°N), the observed PPP is close to the upper bound of model ensembles.

Spatially, the predictability is higher in the tropical regions than in extratropical regions (Figure 1c), such as the most areas of Africa, India, Malay Archipelago, Australia, most areas of South America, and Mexico, consistent with existing studies (G. J. Boer, 2004; Koster et al., 2000; S. Li & Robertson, 2015; Zhu et al., 2014). The higher PPP in the tropics is related to large-scale climate modes such as ENSO (R. Allan et al., 1996; Rasmusson & Wallace, 1983) and MJO (Zhang, 2005). ENSO is the major predictability source of precipitation at seasonal scales in the tropics, while MJO is the largest intraseasonal variability in the tropical atmosphere (B. Kirtman et al., 2013). The precipitation predictability sources in the extratropical areas may include snow, sea ice, and some other large-scale patterns (B. Kirtman et al., 2013). Model simulations exhibit a similar spatial pattern with observations (Figure 1d), although the predictability by the ensemble mean of simulations is larger than observations in some areas such as central Africa.

The spatial patterns of PPP generally show a decreasing trend with the increase of lead time (Figures 1c and 1d). This result is expected because the variance of longer time scale data is generally less than that from shorter time scale (Wilks, 2011). This result also complies with the knowledge that long-lead precipitation forecasts may be less accurate as short-term ones (B. P. Kirtman et al., 2014; Xu et al., 2018). However, this does not necessarily mean that seasonal precipitation is less predictable than daily short-term precipitation. Instead, the decreasing PPP from 2-week to seasonal scales indicates that precipitation variance is more accounted for at 2 weeks than seasonal scale, and 2-week precipitation may be potentially more predictable than seasonal total precipitation (G. Boer & Lambert, 2008).

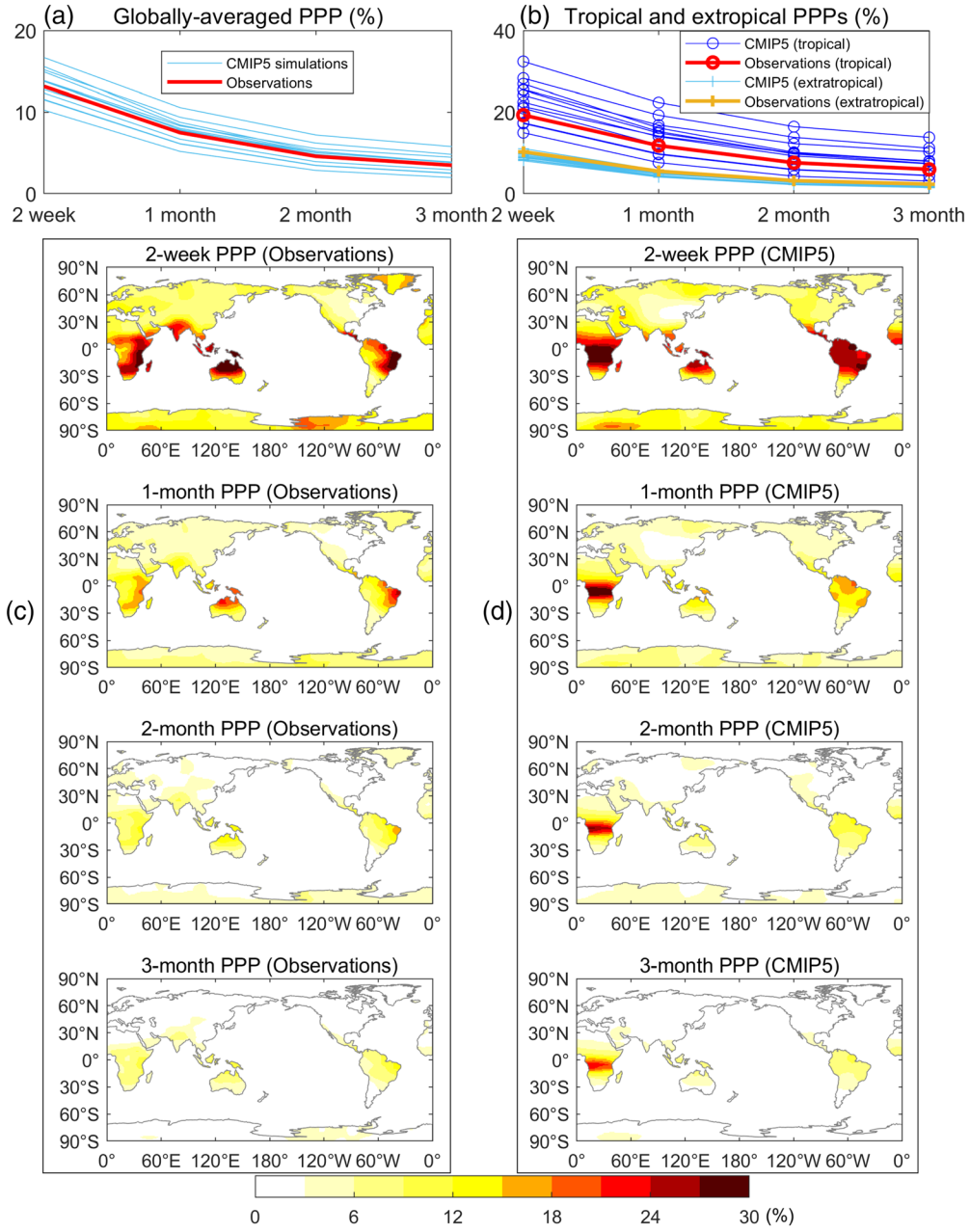

Figure 1. The observed and simulated PPP values at (a) different time scales and (b) different regions. The spatial patterns of observed and simulated PPPs are shown in (c) and (d), respectively, at all the four time scales. The 12 CMIP5 models are used to calculate individual PPP values in Figures 1a and 1b and the average in Figure 1d.

3.2. Predictability Change Under Future Warming

Figure 2 shows the PPP change under future warming scenarios and its connection with SST change. The global median-averaged PPP exhibits a decreasing trend when the warming levels rise from Historical to RCP2.6, RCP4.5, and RCP8.5 (Figure 2a), although the spread is large. The decreasing PPP magnitude is small and very close to each other among the 2-week, 1-month, 2-month, and 3-month scales (Figures 2a and S1). A two-sample *t* test indicates that the PPP changes on a short-term scale and tropics may not be significantly larger than long-term scale and the extratropics at 90% confidence interval (Tables S2 and S3). Although the ensembles show divergent PPP trend at these warming levels, the ensemble mean of these models presents a steady decline, consistent with a previous study (G. Boer, 2009). The decreasing PPP is

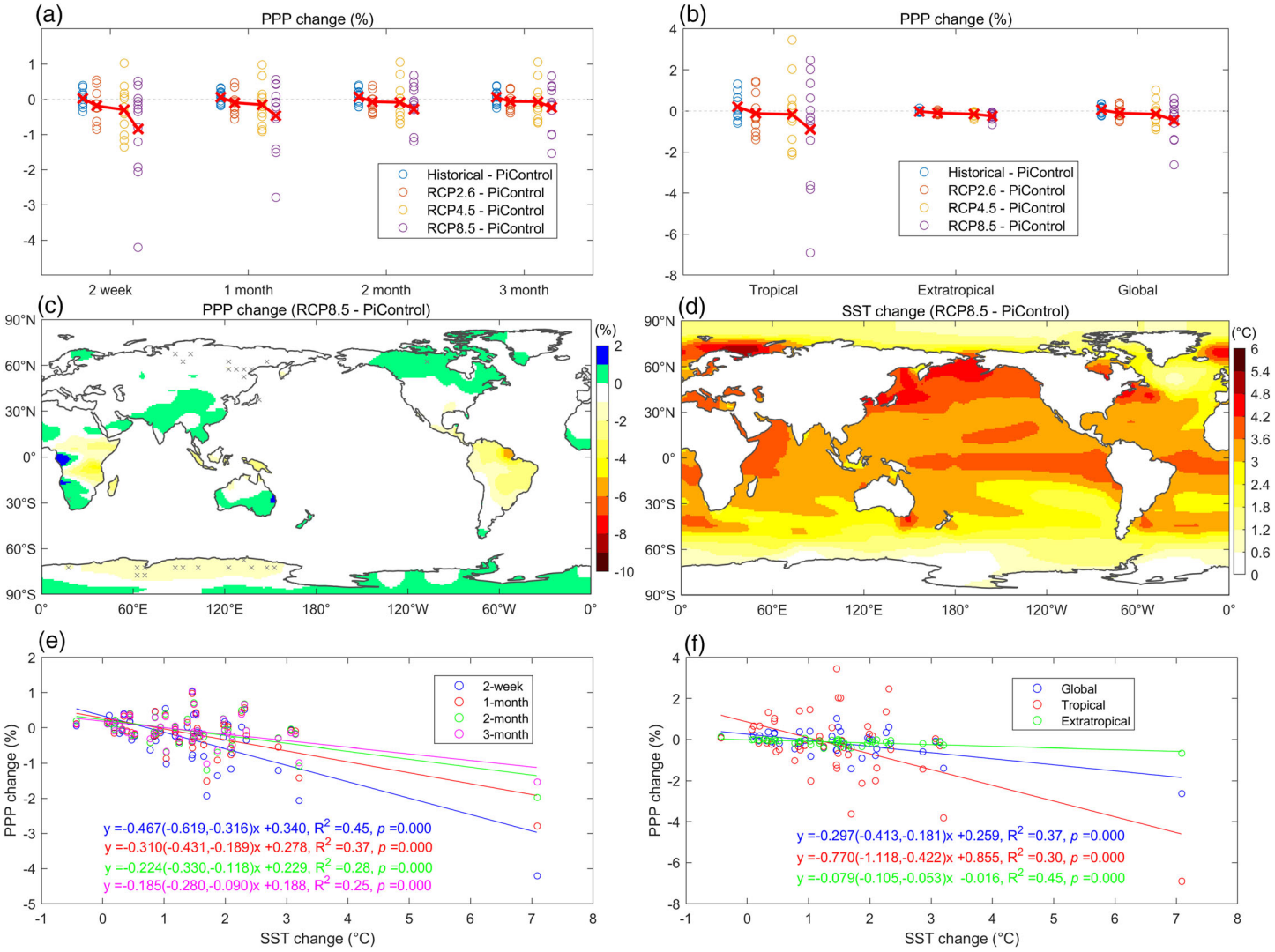

Figure 2. The projected PPP change under future global warming. (a) PPP change on the four time scales. (b) PPP change over tropical, extratropical areas and globally. (c) Spatial patterns of PPP change averaged over all the CMIP5 models and the four time scales. (d) Global SST change. (e) Regression between SST change and PPP change on the four time scales and (f) over different regions averaged over four time scales. The colored points in Figure 2a denote different CMIP5 models, and the line denotes the mean. The "×" symbol in Figure 2c indicates that the PPP change is significant at 90% confidence interval. The predictability ensembles from the CMIP5 models are randomly sampled 1,000 times, and the data range between the 50th and 950th data points after sortation is regarded as the 90% confidence interval. If the predictability change signal within the 90% confidence interval contains zero, the PPP change is not significant and vice versa. The white areas in the world's land of Figure 2c indicate negative PPP change between −1% and 0. The data points in Figures 2e and 2f denote a combination of CMIP5 models and RCP scenarios. A global area-weighted average of SST and PPP changes is used in Figure 2e. The numbers in parenthesis for Figures 2e and 2f denote the 90% confidence interval.

related to the faster changing daily climatological precipitation variance relative to the long-term variance (Figure S2). The increasing daily and long-term precipitation variances are related to the increase in the precipitation events and extremes under water cycle intensification with global warming (Giorgi et al., 2019; Pendergrass et al., 2017; Xu et al., 2019; Yoon et al., 2015; W. Zhang, Zhou, et al., 2019; X. Zhang, Chen, et al., 2019).

Increasing precipitation extremes are related to the change in atmospheric moisture holding capacity with temperature based on the Clausius-Clapeyron (C-C) relationship (Lenderink & Fowler, 2017; Lenderink & van Meijgaard, 2008; Pfahl et al., 2017; Prein et al., 2017). The daily climatological variance is increasing at a faster rate than long-term variance, suggesting that the daily precipitation is becoming more chaotic

than the long-term average. Precipitation variability is closely related to atmospheric moisture content and atmospheric circulation (Gao et al., 2012; Wu et al., 2020), such as moisture flux convergence (MFC), soil moisture, and humidity. MFC can increase atmospheric humidity, enhance the moisture static energy and atmospheric instability, and promote convection (Junquas et al., 2012; Kim & Ha, 2015; Tamoffo et al., 2019; J. Wei et al., 2016). Soil moisture influences the fluxes of heat and moisture originating at the land surface, thus altering atmospheric humidity, temperature, and precipitation (Tuttle & Salvucci, 2016). The variations of MFC, soil moisture, and humidity all contribute to the changing precipitation variability under global warming through local evapotranspiration and remote moisture transport (J. Wei et al., 2016), although these effects may vary with regions.

The PPP change in the tropical areas has a larger model spread than the extratropics under future warming (Figure 2b). As for the spatial patterns, a large fraction of global lands exhibit a decreasing PPP trend (Figure 2c), such as the central and northern Africa, Malay Archipelago, northern Australia, South America, United States, most parts of Asia, and Europe, although the PPP change over most areas is within ±1%. The evident PPP decline is seen in the tropical regions where climatological mean rainfall is high. A slightly increasing PPP is seen in southern Asia, southern Australia, northern North America, southern Africa, and part of Antarctica. The spatial patterns of PPP change may vary greatly among individual models over different regions (Figure S3), especially for eastern and central Africa and northern and eastern South America. The high PPP changes in Tanzania and Guianas among some models (Figure S3) are related to the abnormal precipitation simulations in some years in models after removing the daily climatology. The abnormal precipitation leads to abnormal precipitation variances (Figure S2) as well as the abnormal PPPs (Figure 1) and their changes (Figure S3). There are very few areas with significant PPP change spatially, suggesting divergent model results (Figure 2c).

The ENSO and MJO are the two major large-scale climate modes accounting for the predictability over the tropics. The Pacific ENSO may be more challenging to predict under global warming (Jia et al., 2019), as the ascending over the equatorial Atlantic is weaker due to an increased tropospheric stability in the mean climate, resulting in a weaker impact on the Pacific Ocean. The tropical static stability increases may weaken the MJO's ability to influence extreme events in future warmer climate by weakening wind teleconnections (Bui & Maloney, 2018). Furthermore, the poleward migration of the Hadley Circulation will change the precipitation patterns in the tropics (Mathew & Kumar, 2019; Studholme & Gulev, 2018) and may weaken tropical teleconnections.

The global SST is increasing over global oceans in the RCP8.5 scenario relative to preindustrial time (Figure 2d). Some areas are projected to increase more than 4°C, such as the central and northern Pacific, western Indian Ocean, and central Atlantic. High-latitude areas near the poles exhibit smaller SST increase than the tropics. This spatial SST pattern may seem different from the IPCC report (Pachauri et al., 2014) and is dependent on models. Overall, the global SST is expected to increase under future warming period.

We regressed the SST change and PPP change using a linear model and obtained a coefficient of determination (R^2) of 0.45, 0.37, 0.28, and 0.25 for 2-week, 1-month, 2-month, and 3-month time scales, respectively (Figure 2e). The slopes of regression model for all the four time scales indicate a decreasing trend of PPP with SST increase, and the decrease on short-term time scale is possibly larger than that of long-term scale. Figure 2f demonstrates the regression of PPP change averaged over the four time scales and SST change. The slope of the linear regression model suggests that a −0.8% (−1.1%, −0.4%), −0.08% (−0.1%, −0.05%), and −0.3% (−0.4%, −0.2%) PPP change per 1°C increase in global SST is expected for tropical, extratropical areas and globally, respectively. The PPP decrease is possibly slightly larger for short-term time scales than that of long-term scales (Figure S4). The estimated PPP change trends are similar when removing the extreme SST values beyond 5°C increase in the regression (Figure S5).

3.3. ENSO-Precipitation Correlation, SST Predictability, and Connection With PPP

Figure 3 shows the ENSO-land precipitation correlation change, PSSTP change, and the relationship between PSSTP and PPP. We aim to explore the possible causes influencing PPP change under future warming, especially the SST. Figure 3a plots the changes of land precipitation correlation with ENSO averaged over the four time scales with lags of 2 weeks, 1 month, 2 months, and 3 months under RCP8.5 scenario relative to preindustrial simulations. Here ENSO is represented by the SST anomaly over Niño

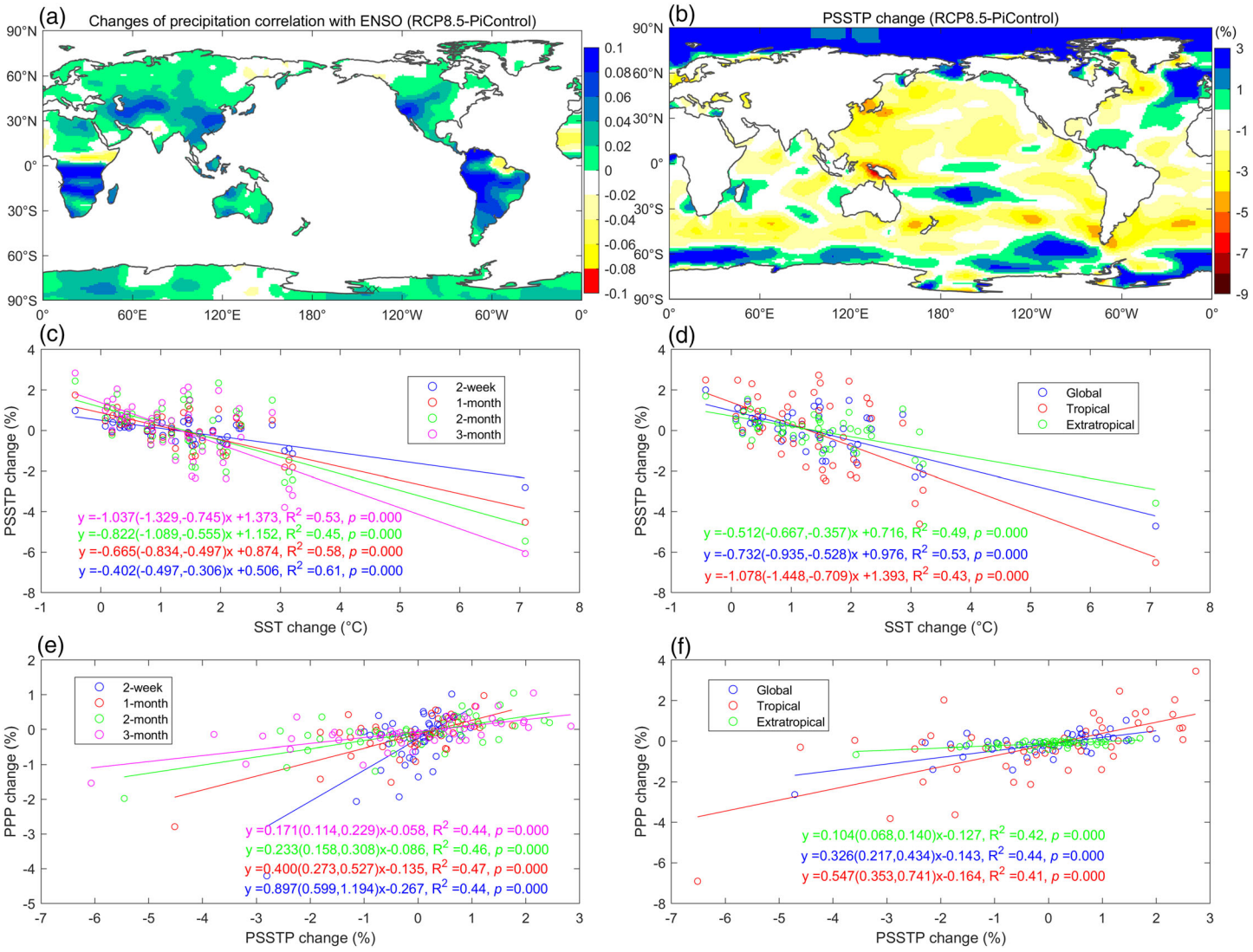

Figure 3. The ENSO-land precipitation correlation change, PSSTP change and connection with PPP under future warming. (a) ENSO-precipitation correlation change. (b) PSSTP change in P3 relative to P1. (c) Regression between SST change and PSSTP change on different time scales and d regions. (e) Regression between PSSTP change and PPP change on different time scales and (f) regions. The ENSO-precipitation lagged correlation is calculated by correlating the Niño 3.4 index and precipitation at 2-week, 1-month, 2-month, and 3-month time scales and then averaging the four scales. The lags are assumed the same as the used time scale. For example, the 2-week correlation is calculated by correlating the ENSO index 2 weeks before the target time and the precipitation at the target time. The "×" symbol in Figures 3a–3b indicates that the result is significant at 90% confidence interval. The significance is calculated the same with that of Figure 2c. The white areas in the world's land of Figure 3a indicate negative correlation change between −0.02 and 0. The white areas in Figure 3b indicate land part, and their PSSTPs are not calculated. The numbers in parenthesis for Figures 3c–3f denote the 90% confidence interval.

3.4 region (5°N to 5°S, 170–120°W). ENSO-related precipitation correlation is increasing over large parts of the world (Figure 3a), indicating possibly enhanced ENSO-induced land precipitation events under future warming (Fasullo et al., 2018; Yeh et al., 2018; Z.–Q. Zhou et al., 2014). The ENSO-land precipitation correlation is divergent among the used CMIP5 models (Figure S6), and there are limited areas exhibiting significant model agreement spatially (Figure 3a), suggesting considerable model uncertainty. However, the enhanced ENSO-land precipitation correlation does not suggest increased precipitation predictability, because ENSO predictability may not increase in a warmer world (Fasullo et al., 2018; Yan et al., 2020).

Figure 3b shows the PSSTP change from P1 to P3 under RCP8.5 scenario. The PSSTP generally decreases with future warming over most ocean basins except the poles, the central Pacific, and some small areas.

However, the insignificant changes in PPP (Figure 2c) and PSSTP (Figures 3b and S7) hinder a robust attribution spatially. The changing PSSTP is probably related to the intensification of oceanic stratification and the acceleration of propagation of Rossby waves (S. Li et al., 2020). Figures 3c and 3d show the linear relationship between PSSTP change and SST change over different time scales and regions, respectively. The PSSTP is likely to decrease when the SST increases, as the slopes of these regressions all show a negative relationship. The decreasing PSSTP magnitude is smaller on short-term time scale than long-term scale (Figure 3c) and is higher in the tropics than that in the extratropics (Figure 3d). Similar results could be seen when removing the extreme high SST values in the regression (Figure S8). Present studies focus more on the SST-forced climate predictability and less on the SST predictability itself (Newman, 2007; Wajsowicz, 2005). The intrinsic physical mechanisms influencing SST predictability need further investigation, such as ocean stratification, SST gradient, entrainment of the mixed layer, and human greenhouse emission.

We regressed the PSSTP change and PPP change to examine their connections as precipitation predictability mainly comes from SST variability. A positive relationship is seen between PPP change and PSSTP change on the four time scales (Figure 3e) and different regions (Figure 3f). When the PSSTP increases, the PPP is likely to increase, despite at a slower rate. A larger impact of PSSTP on PPP is expected on short-term time scale than long-term one and is expected over tropical areas than the extratropics. The statistically significant relationship between PSSTP and PPP indicates a strong impact of SST predictability on precipitation predictability.

We calculated the SST predictability over the Niño 3.4 region to represent the potential ENSO predictability (PENSOP). The relationship between PENSOP change and PPP change is examined using linear regression. The PENSOP change could explain a limited percentage of PPP change (Figure S9). For example, 17% PPP change globally could be explained by PENSOP change at 3-month time scale, and the percentage decreases when the time scale decreases (Figure S9). A 9% PPP change globally could be explained by PENSOP change averaged over the four time scales. The result is expected because ENSO could account for a limited fraction of global precipitation variability (R. Allan et al., 1996; Haszpra et al., 2020; Rasmusson & Wallace, 1983; Westra et al., 2015).

4. Conclusion

The PPP is estimated from CMIP5 simulations using ppvf method over global lands. In the future warming period, the PPP is likely to decrease 0.8%, 0.1%, and 0.3% over tropical, extratropical areas and globally, respectively. Short-term PPP is expected to decrease much more than that in the long-term scale, indicating that short-term precipitation predictability is more likely to be affected by global warming. Despite the divergent model simulations, a general decreasing PPP is projected under future warming based on the multimodel mean. The decreasing PPP poses increasing challenges for weather and climate prediction in the future, especially under the RCP8.5 warming scenario.

The faster increasing daily precipitation variance relative to monthly or seasonal precipitation variance leads to declining PPP, indicating that long-term precipitation variance is less distinguishable from short-term weather noise. The declining PPP under warming indicates a more chaotic and less predictable climate system. PPP decrease is closely related to the decrease of PSSTP, although the ENSO-related precipitation correlation may be enhanced in a warmer climate (Fasullo et al., 2018; Yeh et al., 2018). The ENSO-induced precipitation events are probably less predictable due to decreasing PSSTP. The potential changing ENSO predictability could explain a limited percentage of PPP change.

The decreasing PSSTP and PPP under future warming indicates that SST and precipitation are potentially less predictable when the warming continues. However, the practical predictability is highly dependent on the knowledge of predictability source and models (Mamalakis et al., 2018; Pan et al., 2019; Wang et al., 2015). The predictability could be increased if new predictability sources are found or better model physics are used. Therefore, the PPP results may vary with regions and models. Despite the discrepancy between theoretical and pratical estimations, precipitation predictability is probably decreasing in the future, bringing potentially larger risk and vulnerability to humans, agriculture, and infrastructure exposed to extreme precipitation.

Data Availability Statement

The CMIP5 data are available at the website (https://esgf-node.llnl.gov/projects/cmip5/). The MERRA-2 data are available at the website (https://gmao.gsfc.nasa.gov/reanalysis/MERRA-2/).

Acknowledgments
This work was supported by the National Natural Science Foundation of China Program (41801339 and 41890822), the National Key R&D Program (2018YFB2100500), and the China Scholarship Council (201906270231).

References

Allan, R., Lindesay, J., & Parker, D. (1996). *El Niño Southern Oscillation & climatic variability*. Collingwood, Victoria, Australia: CSIRO publishing.

Allan, R. P., & Soden, B. J. (2008). Atmospheric warming and the amplification of precipitation extremes. *Science*, *321*(5895), 1481–1484. https://doi.org/10.1126/science.1160787

Boer, G. (2009). Changes in interannual variability and decadal potential predictability under global warming. *Journal of Climate*, *22*(11), 3098–3109. https://doi.org/10.1175/2008JCLI2835.1

Boer, G., & Lambert, S. (2008). Multi-model decadal potential predictability of precipitation and temperature. *Geophysical Research Letters*, *35*, L05706. https://doi.org/10.1029/2008GL033234

Boer, G. J. (2004). Long time-scale potential predictability in an ensemble of coupled climate models. *Climate Dynamics*, *23*(1), 29–44. https://doi.org/10.1007/s00382-004-0419-8

Bui, H. X., & Maloney, E. D. (2018). Changes in Madden-Julian Oscillation precipitation and wind variance under global warming. *Geophysical Research Letters*, *45*, 7148–7155. https://doi.org/10.1029/2018GL078504

DelSole, T., Trenary, L., Tippett, M. K., & Pegion, K. (2017). Predictability of week-3–4 average temperature and precipitation over the contiguous United States. *Journal of Climate*, *30*(10), 3499–3512. https://doi.org/10.1175/JCLI-D-16-0567.1

DelSole, T., Yan, X., Dirmeyer, P. A., Fennessy, M., & Altshuler, E. (2014). Changes in seasonal predictability due to global warming. *Journal of Climate*, *27*(1), 300–311. https://doi.org/10.1175/JCLI-D-13-00026.1

Dong, L., Leung, L. R., & Song, F. (2018). Future changes of subseasonal precipitation variability in North America during winter under global warming. *Geophysical Research Letters*, *45*, 12,467–12,476. https://doi.org/10.1029/2018GL079900

Fasullo, J., Otto-Bliesner, B., & Stevenson, S. (2018). ENSO's changing influence on temperature, precipitation, and wildfire in a warming climate. *Geophysical Research Letters*, *45*, 9216–9225. https://doi.org/10.1029/2018GL079022

Gao, Y., Leung, L. R., Salathé, E. P. Jr., Dominguez, F., Nijssen, B., & Lettenmaier, D. P. (2012). Moisture flux convergence in regional and global climate models: Implications for droughts in the southwestern United States under climate change. *Geophysical Research Letters*, *39*, L09711. https://doi.org/10.1029/2012GL051560

Gelaro, R., McCarty, W., Suárez, M. J., Todling, R., Molod, A., Takacs, L., et al. (2017). The modern-era retrospective analysis for research and applications, version 2 (MERRA-2). *Journal of Climate*, *30*(14), 5419–5454. https://doi.org/10.1175/JCLI-D-16-0758.1

Giorgi, F., Raffaele, F., & Coppola, E. (2019). The response of precipitation characteristics to global warming from climate projections. *Earth System Dynamics*, *10*(1), 73–89. https://doi.org/10.5194/esd-10-73-2019

Hao, Z., AghaKouchak, A., Nakhjiri, N., & Farahmand, A. (2014). Global integrated drought monitoring and prediction system. *Scientific Data*, *1*, 140001. https://doi.org/10.1038/sdata.2014.1

Hartmann, H., Snow, J. A., Su, B., & Jiang, T. (2016). Seasonal predictions of precipitation in the Aksu-Tarim River basin for improved water resources management. *Global and Planetary Change*, *147*, 86–96. https://doi.org/10.1016/j.gloplacha.2016.10.018

Haszpra, T., Herein, M., & Bódai, T. (2020). Investigating ENSO and its teleconnections under climate change in an ensemble view—A new perspective. *Earth System Dynamics*, *11*(1), 267–280. https://doi.org/10.5194/esd-11-267-2020

Jia, F., Cai, W., Wu, L., Gan, B., Wang, G., Kucharski, F., et al. (2019). Weakening Atlantic Niño–Pacific connection under greenhouse warming. *Science Advances*, *5*(8), eaax4111. https://doi.org/10.1038/d41586-019-02362-5

Jiang, M., Felzer, B. S., & Sahagian, D. (2016). Predictability of precipitation over the conterminous U.S. based on the CMIP5 multi-model ensemble. *Scientific Reports*, *6*(1), 29962. https://doi.org/10.1038/srep29962

Junquas, C., Vera, C., Li, L., & Le Treut, H. (2012). Summer precipitation variability over Southeastern South America in a global warming scenario. *Climate Dynamics*, *38*(9–10), 1867–1883. https://doi.org/10.1007/s00382-011-1141-y

Kang, I.-S., Lee, J.-Y., & Park, C.-K. (2004). Potential predictability of summer mean precipitation in a dynamical seasonal prediction system with systematic error correction. *Journal of Climate*, *17*(4), 834–844. https://doi.org/10.1175/1520-0442(2004)017<0834:PPOSMP>2.0.CO;2

Kim, B.-H., & Ha, K.-J. (2015). Observed changes of global and western Pacific precipitation associated with global warming SST mode and mega-ENSO SST mode. *Climate Dynamics*, *45*(11–12), 3067–3075. https://doi.org/10.1007/s00382-015-2524-2

Kirtman, B., Power, S. B., Adedoyin, A. J., Boer, G. J., Bojariu, R., Camilloni, I., et al. (2013). Near-term climate change: Projections and predictability.

Kirtman, B. P., Min, D., Infanti, J. M., Kinter, J. L. III, Paolino, D. A., Zhang, Q., et al. (2014). The North American multimodel ensemble: Phase-1 seasonal-to-interannual prediction; phase-2 toward developing intraseasonal prediction. *Bulletin of the American Meteorological Society*, *95*(4), 585–601. https://doi.org/10.1175/BAMS-D-12-00050.1

Koster, R. D., Suarez, M. J., & Heiser, M. (2000). Variance and predictability of precipitation at seasonal-to-interannual timescales. *Journal of Hydrometeorology*, *1*(1), 26–46. https://doi.org/10.1175/1525-7541(2000)001<0026:VAPOPA>2.0.CO;2

Lenderink, G., & Fowler, H. J. (2017). Understanding rainfall extremes. *Nature Climate Change*, *7*(6), 391–393. https://doi.org/10.1038/nclimate3305

Lenderink, G., & van Meijgaard, E. (2008). Increase in hourly precipitation extremes beyond expectations from temperature changes. *Nature Geoscience*, *1*(8), 511–514. https://doi.org/10.1038/ngeo262

Li, S., & Robertson, A. W. (2015). Evaluation of submonthly precipitation forecast skill from global ensemble prediction systems. *Monthly Weather Review*, *143*(7), 2871–2889. https://doi.org/10.1175/MWR-D-14-00277.1

Li, S., Wu, L., Yang, Y., Geng, T., Cai, W., Gan, B., et al. (2020). The Pacific Decadal Oscillation less predictable under greenhouse warming. *Nature Climate Change*, *10*(1), 30–34. https://doi.org/10.1038/s41558-019-0663-x

Liu, T., Schmitt, R., & Li, L. (2018). Global search for autumn-lead sea surface salinity predictors of winter precipitation in southwestern United States. *Geophysical Research Letters*, *45*, 8445–8454. https://doi.org/10.1029/2018GL079293

Lou, J., Holbrook, N. J., & O'Kane, T. J. (2019). South Pacific decadal climate variability and potential predictability. *Journal of Climate*, *32*(18), 6051–6069. https://doi.org/10.1175/JCLI-D-18-0249.1

Luo, J.-J., Behera, S. K., Masumoto, Y., & Yamagata, T. (2010). Impact of global ocean surface warming on seasonal-to-interannual climate prediction. *Journal of Climate*, *24*(6), 1626–1646. https://doi.org/10.1175/2010jcli3645.1
Maloney, E. D., & Kiehl, J. T. (2002). MJO-related SST variations over the tropical eastern Pacific during Northern Hemisphere summer. *Journal of Climate*, *15*(6), 675–689. https://doi.org/10.1175/1520-0442(2002)015<0675:MRSVOT>2.0.CO;2
Mamalakis, A., Yu, J.-Y., Randerson, J. T., AghaKouchak, A., & Foufoula-Georgiou, E. (2018). A new interhemispheric teleconnection increases predictability of winter precipitation in southwestern US. *Nature Communications*, *9*(1), 1–10. https://doi.org/10.1038/s41467-018-04722-7
Mathew, S. S., & Kumar, K. K. (2019). Characterization of the long-term changes in moisture, clouds and precipitation in the ascending and descending branches of the Hadley circulation. *Journal of Hydrology*, *570*, 366–377. https://doi.org/10.1016/j.jhydrol.2018.12.047
Newman, M. (2007). Interannual to decadal predictability of tropical and north Pacific sea surface temperatures. *Journal of Climate*, *20*(11), 2333–2356. https://doi.org/10.1175/JCLI4165.1
Pachauri, R. K., Allen, M. R., Barros, V. R., Broome, J., Cramer, W., Christ, R., et al. (2014). Climate change 2014: Synthesis report. Contribution of working groups I. *II and III to the fifth assessment report of the Intergovernmental Panel on Climate Change*, IPCC.
Pan, X., Wang, G., & Yang, P. (2019). Introducing driving-force information increases the predictability of the North Atlantic Oscillation. *Atmospheric and Oceanic Science Letters*, *12*(5), 329–336. https://doi.org/10.1080/16742834.2019.1628608
Papacharalampous, G., Tyralis, H., & Koutsoyiannis, D. (2018). Predictability of monthly temperature and precipitation using automatic time series forecasting methods. *Acta Geophysica*, *66*(4), 807–831. https://doi.org/10.1007/s11600-018-0120-7
Pendergrass, A. G., Knutti, R., Lehner, F., Deser, C., & Sanderson, B. M. (2017). Precipitation variability increases in a warmer climate. *Scientific Reports*, *7*(1), 1–9. https://doi.org/10.1038/s41598-017-17966-y
Pfahl, S., O'Gorman, P. A., & Fischer, E. M. (2017). Understanding the regional pattern of projected future changes in extreme precipitation. *Nature Climate Change*, *7*(6), 423–427. https://doi.org/10.1038/nclimate3287
Prein, A. F., Rasmussen, R. M., Ikeda, K., Liu, C., Clark, M. P., & Holland, G. J. (2017). The future intensification of hourly precipitation extremes. *Nature Climate Change*, *7*(1), 48–52. https://doi.org/10.1038/nclimate3168
Rasmusson, E. M., & Wallace, J. M. (1983). Meteorological aspects of the El Nino/Southern Oscillation. *Science*, *222*(4629), 1195–1202. https://doi.org/10.1126/science.222.4629.1195
Scher, S., & Messori, G. (2019). How global warming changes the difficulty of synoptic weather forecasting. *Geophysical Research Letters*, *46*, 2931–2939. https://doi.org/10.1029/2018GL081856
Silvestro, F., & Rebora, N. (2014). Impact of precipitation forecast uncertainties and initial soil moisture conditions on a probabilistic flood forecasting chain. *Journal of Hydrology*, *519*, 1052–1067. https://doi.org/10.1016/j.jhydrol.2014.07.042
Studholme, J., & Gulev, S. (2018). Concurrent changes to Hadley circulation and the meridional distribution of tropical cyclones. *Journal of Climate*, *31*(11), 4367–4389. https://doi.org/10.1175/JCLI-D-17-0852.1
Tamoffo, A. T., Moufouma-Okia, W., Dosio, A., James, R., Pokam, W. M., Vondou, D. A., et al. (2019). Process-oriented assessment of RCA4 regional climate model projections over the Congo Basin under 1.5°C and 2°C global warming levels: Influence of regional moisture fluxes. *Climate Dynamics*, *53*(3–4), 1911–1935. https://doi.org/10.1007/s00382-019-04751-y
Taylor, K. E., Stouffer, R. J., & Meehl, G. A. (2012). An overview of CMIP5 and the experiment design. *Bulletin of the American Meteorological Society*, *93*(4), 485–498. https://doi.org/10.1175/BAMS-D-11-00094.1
Tuttle, S., & Salvucci, G. (2016). Empirical evidence of contrasting soil moisture-precipitation feedbacks across the United States. *Science*, *352*(6287), 825–828. https://doi.org/10.1126/science.aaa7185
Wajsowicz, R. C. (2005). Potential predictability of tropical Indian Ocean SST anomalies. *Geophysical Research Letters*, *32*, L24702. https://doi.org/10.1029/2005GL024169
Wang, B., Xiang, B., Li, J., Webster, P. J., Rajeevan, M. N., Liu, J., & Ha, K.-J. (2015). Rethinking Indian monsoon rainfall prediction in the context of recent global warming. *Nature Communications*, *6*(1), 7154. https://doi.org/10.1038/ncomms8154
Wei, J., Su, H., & Yang, Z.-L. (2016). Impact of moisture flux convergence and soil moisture on precipitation: A case study for the southern United States with implications for the globe. *Climate Dynamics*, *46*(1–2), 467–481. https://doi.org/10.1007/s00382-015-2593-2
Wei, W., Yan, Z., & Jones, P. (2017). Potential predictability of seasonal extreme precipitation accumulation in China. *Journal of Hydrometeorology*, *18*(4), 1071–1080. https://doi.org/10.1175/JHM-D-16-0141.1
Westra, S., Renard, B., & Thyer, M. (2015). The ENSO—Precipitation teleconnection and its modulation by the interdecadal Pacific oscillation. *Journal of Climate*, *28*(12), 4753–4773. https://doi.org/10.1175/JCLI-D-14-00722.1
Westra, S., & Sharma, A. (2010). An upper limit to seasonal rainfall predictability? *Journal of Climate*, *23*(12), 3332–3351. https://doi.org/10.1175/2010JCLI3212.1
Wheeler, M. C., Zhu, H., Sobel, A. H., Hudson, D., & Vitart, F. (2017). Seamless precipitation prediction skill comparison between two global models. *Quarterly Journal of the Royal Meteorological Society*, *143*(702), 374–383. https://doi.org/10.1002/qj.2928
Wilks, D. S. (2011). *Statistical methods in the atmospheric sciences*. Oxford: Academic press.
Wu, J., Han, Z., Xu, Y., Zhou, B., & Gao, X. (2020). Changes in extreme climate events in China under 1.5°C–4°C global warming targets: Projections using an ensemble of regional climate model simulations. *Journal of Geophysical Research: Atmospheres*, *125*, e2019JD031057. https://doi.org/10.1029/2019JD031057
Xu, L., Chen, N., Moradkhani, H., Zhang, X., & Hu, C. (2020). Improving global monthly and daily precipitation estimation by fusing gauge observations, remote sensing and reanalysis datasets. *Water Resources Research*, *56*, e2019WR026444. https://doi.org/10.1029/2019WR026444
Xu, L., Chen, N., & Zhang, X. (2019). Global drought trends under 1.5 and 2°C warming. *International Journal of Climatology*, *39*(4), 2375–2385. https://doi.org/10.1002/joc.5958
Xu, L., Chen, N., Zhang, X., & Chen, Z. (2018). An evaluation of statistical, NMME and hybrid models for drought prediction in China. *Journal of Hydrology*, *566*, 235–249. https://doi.org/10.1016/j.jhydrol.2018.09.020
Yan, Z., Wu, B., Li, T., Collins, M., Clark, R., Zhou, T., et al. (2020). Eastward shift and extension of ENSO-induced tropical precipitation anomalies under global warming. *Science Advances*, *6*(2), eaax4177. https://doi.org/10.1126/sciadv.aax4177
Yeh, S. W., Cai, W., Min, S. K., McPhaden, M. J., Dommenget, D., Dewitte, B., et al. (2018). ENSO atmospheric teleconnections and their response to greenhouse gas forcing. *Reviews of Geophysics*, *56*(1), 185–206. https://doi.org/10.1002/2017RG000568
Yoon, J.-H., Wang, S. S., Gillies, R. R., Kravitz, B., Hipps, L., & Rasch, P. J. (2015). Increasing water cycle extremes in California and in relation to ENSO cycle under global warming. *Nature Communications*, *6*(1), 1–6. https://doi.org/10.1038/ncomms9657
Zhang, C. (2005). Madden-julian oscillation. *Reviews of Geophysics*, *43*, RG2003. https://doi.org/10.1029/2004RG000158
Zhang, W., Zhou, T., Zhang, L., & Zou, L. (2019). Future intensification of the water cycle with an enhanced annual cycle over global land monsoon regions. *Journal of Climate*, *32*(17), 5437–5452. https://doi.org/10.1175/JCLI-D-18-0628.1

Zhang, X., Chen, N., Sheng, H., Ip, C., Yang, L., Chen, Y., et al. (2019). Urban drought challenge to 2030 sustainable development goals. *Science of the Total Environment*, *693*, 133536. https://doi.org/10.1016/j.scitotenv.2019.07.342

Zhou, X., & Khairoutdinov, M. F. (2017). Changes in temperature and precipitation extremes in superparameterized CAM in response to warmer SSTs. *Journal of Climate*, *30*(24), 9827–9845. https://doi.org/10.1175/JCLI-D-17-0214.1

Zhou, Z.-Q., Xie, S.-P., Zheng, X.-T., Liu, Q., & Wang, H. (2014). Global warming–induced changes in El Niño teleconnections over the North Pacific and North America. *Journal of Climate*, *27*(24), 9050–9064. https://doi.org/10.1175/JCLI-D-14-00254.1

Zhu, H., Wheeler, M. C., Sobel, A. H., & Hudson, D. (2014). Seamless precipitation prediction skill in the tropics and extratropics from a global model. *Monthly Weather Review*, *142*(4), 1556–1569. https://doi.org/10.1175/MWR-D-13-00222.1